Proceedings of the 17th World Congress
The International Federation of Automatic Control
Seoul, Korea, July 6-11, 2008

A Self Servo Writing Scheme for a MEMS Storage Device with Sub-nanometer Precision

Abu Sebastian * **Angeliki Pantazi** * **S. O. Reza Moheimani** **
Haris Pozidis * **Evangelos Eleftheriou** *

* *IBM Zurich Research Laboratory, Rüschlikon, CH-8803 Switzerland*
** *School of Electrical Engineering and Computer Science, University of Newcastle, Australia*

Abstract: In the probe-based storage concept being pursued by IBM, a MEMS based micro-scanner is used to position the storage medium relative to the read/write probes. To achieve repeatable positioning over a large storage area, it is necessary to have medium-derived position information. Dedicated servo-fields are typically employed to obtain medium-derived position information. Sub-nanometer positioning resolutions are desirable while writing these servo-fields. Such precise positioning at acceptable bandwidth using a global position sensor requires the directed design of the closed-loop noise sensitivity transfer function so as to minimize the impact of sensing noise. This paper describes one such control architecture based on resonant controllers where the impact of measurement noise on positioning is minimal while providing sufficient damping and hence satisfactory tracking performance. It is estimated that the positioning error due to sensing noise is a remarkably low 0.25 nm. Experimental results are also presented that show error-free operation of the device at high densities.

1. INTRODUCTION

A probe-storage device uses nanometer-sharp tips, typically used in scanning probe microscopes, to write information to and read the recorded information from a storage medium. Such a technology can be regarded as a natural candidate for overcoming the physical limits on achievable areal density in conventional storage technologies. One implementation of a probe-based storage device is presented in Eleftheriou et al. [2003]. This device is based on a thermo-mechanical principle for storing and retrieving information written on thin polymer films. Digital information is stored by making indentations on the thin polymer film by using the tips of AFM micro-cantilevers, which are a few nanometers in diameter. Ultra-high positioning accuracies are desired for satisfactory error-rate performance. Displacement of the storage medium relative to the array of micro-cantilevers is achieved by means of a silicon-based micro-scanner with x/y-motion capability (see Lantz et al. [2007]).

The global x/y-positional information of the micro-scanner is provided by thermal position sensors (see Lantz et al. [2005]). However, for absolute positioning in a 100 μm $\times$ 100 μm storage field with nanometer-scale resolution, we require some form of media-derived position information besides the thermal position sensors. A feedback-control scheme relying on the thermal sensors alone is not suitable for long-term operation of the device. Because of the availability of multiple probes, a small number of probes and their respective storage fields are dedicated for the generation of medium-derived position information. Prior to using a MEMS-based scanning-probe storage device, the servo information generating the medium-derived position information has to be written in the storage fields reserved for this specific purpose. This operation is referred to as "servo writing". Note, that unlike in hard disk drives, the servo information is written without assistance from an external positioning device. Hence, it is usually called "self servo writing". Sub-nanometer scale positioning accuracies are desired while performing "self servo write" operation because the positioning errors incurred while writing the servo fields would appear as sensing noise while performing regular read/write operation of the device. Open loop operation is not possible primarily because of the lightly damped poles of the micro-scanner. Conventional feedback controllers on the other hand would make the system sensitive to measurement noise, particularly the low-frequency components and sensor drift.

In controlling a dynamical system, it is imperative that frequency regions exist in which "control is essential", e.g., the resonance frequency region in the case of the micro-scanner. It is also evident that in these frequency regions, the closed-loop system would be sensitive to measurement noise. However it is highly desirable and as shown in this paper, possible to carefully design the noise sensitivity transfer function such that the closed-loop system is insensitive to measurement noise outside these frequency regions. What makes this possible is the fact that the device is operated in a vibration free environment during the "self servo write" process and that the closed-loop system has no disturbance rejection objective. In nanopositioning applications that require positioning errors to be well below the resolution provided by the position sensors, a directed shaping of the noise sensitivity transfer function is essential. One approach can be to use H_∞ or H_2 optimal control formulations. However, it turns out that a resonant controller provides us with the desired noise sensitivity transfer function. A resonant controller has a simple structure, is easy to implement, and guarantees closed-loop stability in the presence of out-of-bandwidth dynamics. In this paper we illustrate the concept of noise sensitivity transfer function shaping using a resonant controller architecture for the "self servo write" application.

2. THE STORAGE DEVICE

The schematic of the probe-based data-storage prototype system is shown in Figure 1. To position the storage medium relative to the cantilever array, a miniaturized scanner is used

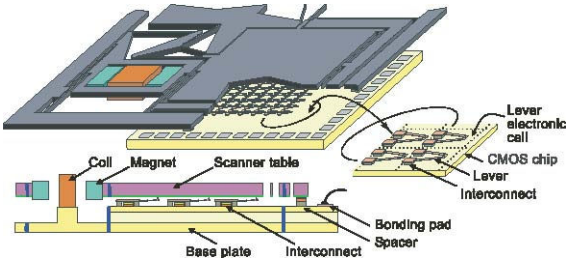

Fig. 1. Schematic of MEMS-based probe-storage device. Reprinted from Eleftheriou et al. [2003]. (c) 2003 IEEE

with x/y-motion capabilities that are on the order of the pitch between the micro-cantilevers in the array. The scan table, which carries the polymer storage medium, can be displaced in two orthogonal directions (x and y) in the plane of the silicon wafer.

Two pairs of thermal position sensors are used to provide the x/y-position information of the micro-scanner. Thermal position sensors are micro-heaters that form part of the chip holding the cantilever array. They are placed in such a way that they partially overlap the scan table. As the scanner moves, there is a change in the overlap between the sensors and the scan table, which results in a change in the temperature. This change in temperature is detected electrically owing to the resulting change in the electrical resistance. These sensors are remarkably linear over the travel range of the micro-scanner and have resolutions of approx. 1nm 1σ over the sensing bandwidth of approx. 5 kHz.

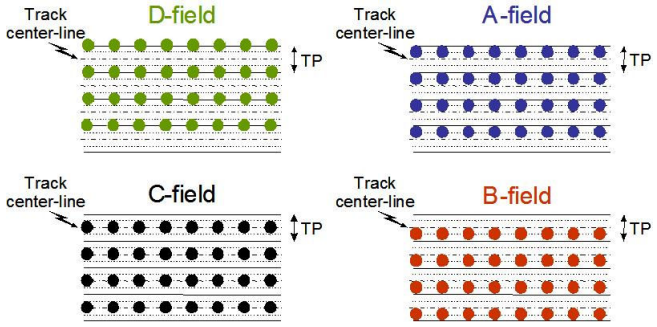

Fig. 2. Servo-burst configuration

Next we describe the medium-derived positional information, the generation of which requires the "self-servo write" process. The method to generate the medium-derived position error signal (PES) is based on the concept of mutually vertically displaced sequences of indentations (bursts), arranged in such a way as to produce two signals in quadrature, which can be combined to provide a robust PES (see Pantazi et al. [2007]). A few storage fields along with their respective cantilevers are dedicated for this purpose. Medium-derived PES can be generated using the servo burst configuration illustrated in Fig. 2, where the circles represent written indentations. Prior to the operation of the device, A, B, C and D bursts are written using the "self-servo" write process in four different dedicated storage fields, called servo fields. The cross-track distance between indentation centers of the same burst is equal to the track pitch (TP), whereas the distance between indentation centers in A and B (or C and D) bursts is TP/2. The distance between A and C centers is TP/4. During the operation of the device, data would be written such that they are aligned to the center of C burst. During writing and reading of the device, the cantilevers associated with the servo fields would always be reading. Any deviation of the data probes from their specified track centers can be detected from a combination of the read-back signals from the four servo fields. The medium-derived PES provides y-positional information around each track centerline and therefore has a maximum range of TP.

3. IDENTIFICATION AND MODELLING

The motion of the micro-scanner in each direction is captured by the linear dynamic components, P_{xx} and P_{yy}. Specifically, the transfer function P_{xx} relates the coil current (u_x in mA) to the output displacement x (in μm) and the transfer function P_{yy} relates the coil current u_y to the output displacement y. The cross-coupling between the axes is modelled as the sum of the linear dynamic components, P_{xy} and P_{yx}, with the memoryless nonlinear functions of the scanner position x and y, $f(x,y)$ and $g(x,y)$, respectively. However, the linear dynamic components of P_{xy} and P_{yx}, are found to be relatively small compared to the nonlinear components in the frequency region of interest.

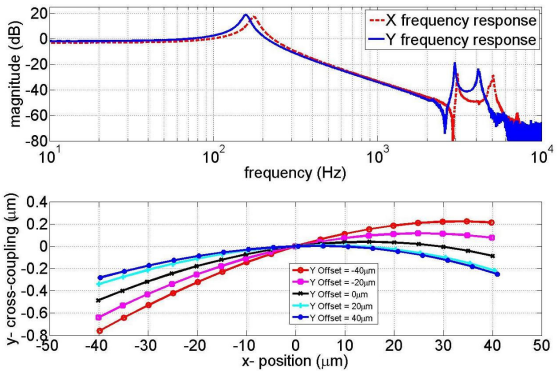

Fig. 3. The experimentally obtained frequency response of the scanner motion in the x- and y-directions as measured by the sensor and cross-coupling between the x- and y-axes.

To identify the transfer functions P_{xx} and P_{yy}, the frequency responses of the scanner in the x- and y-directions are obtained using the thermal position sensors over the range from 1 Hz to 10 kHz. Frequency responses of x- and y-scanner axes are shown in Fig. 3. As can be seen, the dynamics is dominated by the first mode, which can be accurately captured by a simple mass-spring-damper second-order model. The second-order model does not, however, fully describe the behavior of the micro-scanner in the higher-frequency regime, where it exhibits higher-order resonance modes. Figure 3 also shows the cross-coupling on the y-axis due to x-motion for various values of displacement in the y-direction.

The thermal-position sensor bandwidth is determined by the thermo-electric response of the heaters. Typically, a first-order response with a time constant of around 60 to 100 μs accurately captures the sensor dynamics. Positioning accuracy is related to the intrinsic noise characteristics of the sensors. The total measurement noise consists of the thermal-position sensor noise and the quantization noise from the 16-bit ADCs used. The standard deviation of the combined noise has been measured to be 0.97 nm over 10 kHz bandwidth for the x- sensor and 1.00 nm for the y- sensor. Although the accuracy of the sensor is good, there is a significant low-frequency component as can be seen from the power spectral density of the sensor noise shown in Fig. 4. Moreover these sensors are susceptible to drift.

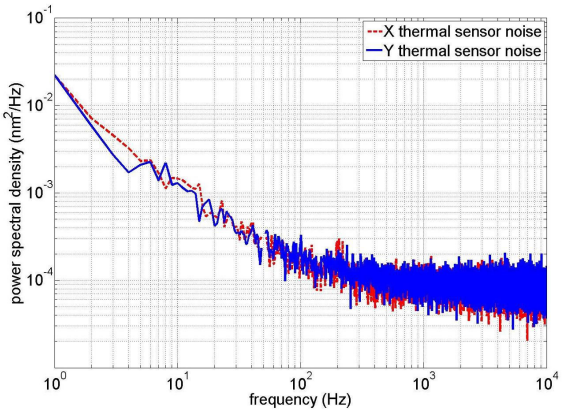

Fig. 4. Measured power spectral density of thermal-sensor noise.

4. CONTROLLER DESIGN FOR SELF SERVO WRITING

During the self servo writing operation, only thermal position sensors are available to provide position information. The tolerable positioning error is well below the resolution of the thermal position sensors. Hence, as discussed earlier, the control design should be such that the closed-loop system is sensitive to measurement noise only in those frequency regions where control is essential. In this section we illustrate that a resonant-controller-based architecture satisfies this condition, thus appropriately shaping the closed-loop noise sensitivity transfer function. The control architectures for the x- and y-scan directions are discussed in this section. However owing to the cross-coupling between the two scan axes, additional steps are required in the design of a control architecture for the y-scan direction.

From the discussions in the previous section, it can be deduced that the dynamics of the micro-scanner along x- and y-directions can be modeled as

$$P_{xx}(s) = \frac{\alpha_{xx}\omega_{xx}^2}{s^2 + 2\zeta_{xx}\omega_{xx}s + \omega_{xx}^2} + \Delta_{xx}(s) \tag{1}$$

and

$$P_{yy}(s) = \frac{\alpha_{yy}\omega_{yy}^2}{s^2 + 2\zeta_{yy}\omega_{yy}s + \omega_{yy}^2} + \Delta_{yy}(s), \tag{2}$$

respectively, where all the parameters are shown in Table 1(a). Furthermore, Δ_{xx} and Δ_{yy} represent the high-frequency resonances of the micro-scanner, which tend to vary as a function of the micro-scanner position.

	xx	yy
α	0.7	0.8
ζ	0.0484	0.0388
ω	1108.5	983.4

(a) Parameters of P_{xx} and P_{yy}

	xx	yy
$\gamma\tilde{\omega}^2$	3.0	3.0
δ	1.1	1.1
$\tilde{\omega}$	1108.5	983.4

(b) Parameters of K_x and K_y

Table 1.

Considering the second-order terms in P_{xx} and P_{yy}, which correspond to the first resonant mode of the micro-scanner along x- and y-directions, it is clear that both transfer functions represent collocated systems. One approach to efficiently damp a collocated system is to use a resonant controller. Resonant controllers have been shown to be very efficient in terms of adding damping to flexible structures with collocated sensors and actuators (see Moheimani and Vautier [2005], Pota et al. [2002], Halim and Moheimani [2001]). They have a very simple structure, do not require a higher bandwidth than the system being controlled, and can guarantee closed-loop stability in the presence of out-of-bandwidth dynamics. However, what makes resonant controllers particularly attractive for our application is the performance of these controllers with respect to measurement noise.

For a single-mode, SISO system, a resonant controller is defined as

$$K(s) = \frac{\gamma\tilde{\omega}^2 s^2}{s^2 + 2\delta\tilde{\omega}s + \tilde{\omega}^2} \tag{3}$$

A resonant controller can be designed in a number of ways. It is possible to minimize a cost function, such as H_2, or the H_∞ norm of the system as a function of controller parameters. However, because of their simple structure, it is usually possible to design a resonant controller by inspection. In particular for collocated SISO systems with low modal density this approach generally works quite well. Here, the resonant controllers, $K_x(s)$ and $K_y(s)$, were designed by inspection to control the micro-scanner's motion along the x- and y-axes, respectively. Controller parameters are tabulated in Table 1 (b).

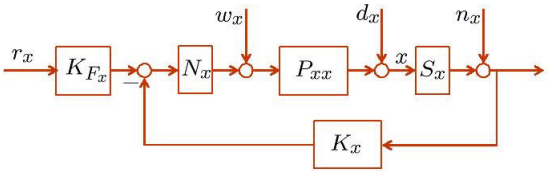

Fig. 5. Block diagram describing the feedback loop for the x-direction.

The block diagram describing the feedback loop for the x- axis is illustrated in Figure 5. In this figure, r_x is the set-point (a triangular waveform for the x-loop), w_x represents the input disturbance signals to the plant, namely, shocks and vibrations and actuator noise, d_x represents output disturbance signals, and n_x represents the sensor noise. The position of the micro-scanner in the x-direction is determined via

$$x = T_{xr}(s)r_x + T_{xd}(s)d_x + T_{xn}(s)n_x + T_{xw}(s)w_x \tag{4}$$

where

$$T_{xr}(s) = \frac{K_{F_x}(s)N_x(s)P_{xx}(s)}{1 + K_x(s)N_x(s)P_{xx}(s)S_x(s)} \tag{5}$$

$$T_{xn}(s) = \frac{-K_x(s)N_x(s)P_{xx}(s)}{1 + K_x(s)N_x(s)P_{xx}(s)S_x(s)} \tag{6}$$

$$T_{xd}(s) = \frac{1}{1 + K_x(s)N_x(s)P_{xx}(s)S_x(s)} \tag{7}$$

$$T_{xw}(s) = \frac{P_{xx}(s)}{1 + K_x(s)N_x(s)P_{xx}(s)S_x(s)}. \tag{8}$$

Here, $N_x(s)$ represents a set of notch filters centered at the out-of-bandwidth resonances of the micro-scanner. These notch filters are incorporated into the feed-forward loop to minimize the effect of the two out-of-bandwidth resonances on the feedback controlled system. Inclusion of these notch filters will make the closed-loop performance of the system less sensitive to Δ_x and Δ_y. The feedforward block, K_{F_x} is just a gain equivalent to the inverse of the DC gain of $P_{xx}(s)$. Furthermore, $S_x(s)$ represents the low-pass dynamics of the thermal sensors.

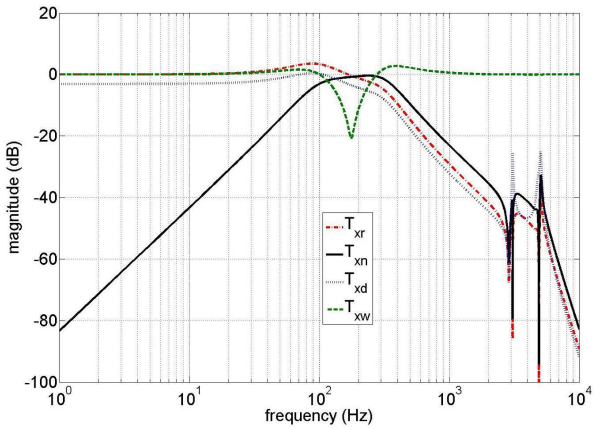

Fig. 6. Closed-loop transfer functions corresponding to the x-axis.

Figure 6 shows the magnitude response of transfer functions $T_{xr}(s)$, $T_{xn}(s)$, $T_{xd}(s)$ and $T_{xw}(s)$. All of the closed-loop transfer functions display a sharp damping at and close to the resonance frequency of the micro-scanner. This is clearly due to the control action. The noise transfer function, $T_{xn}(s)$, has a band-pass profile, centered at the first resonance frequency of the micro-scanner with a 40 dB per decade roll off at low- and high-frequency regions. This is the desired noise sensitivity transfer function. Clearly the sensitivity of measurement noise is limited to the frequency region where control over the dynamics is essential, i.e. the resonance frequency and its vicinity. Moreover as evident from Figure 4, the thermal sensor measurements are particularly noisy at low frequencies. The shape of $T_{xn}(s)$ ensures that the closed-loop system will not suffer significantly from sensor noise, drift, and other low-frequency noises that the micro-scanner can be subject to. The immunity to drift is particularly important. This stems from the fact that $K_x(s)$ has a double zero at the origin, which substantially reduces the effect of low-frequency sensor noise on the operation of the feedback loop. Furthermore, any high-frequency measurement noise is also heavily filtered out. In other words, apart from adding damping to the micro-scanner, the controller reduces the effect of sensor noise on the position of the micro-scanner to an absolute minimum. The price that is paid is in terms of T_{xd} and T_{xw}.

The closed-loop system is very sensitive to input and output disturbances. In particular, low- and high-frequency output disturbances directly affect the position of micro-scanner. However, the feedback loop is reasonably immune to high-frequency input disturbances. To this end, it should be reiterated that input and output disturbances do not pose a significant problem as the self servo writing operation is performed in a controlled vibration-free environment, where the effect of such disturbances is reduced to an absolute minimum. The y-axis feedback loop, as depicted in Figure 7, is very similar to the x-axis loop. It contains a resonant controller tuned to ω_y, and notch filters tuned to the out-of-bandwidth resonant modes of the micro-scanner in the y- axis. Its function, however, is rather different. The reference signal for the y- direction, r_y, is fixed for each period of the triangular signal applied to r_x. This is to facilitate the task of self servo writing over a straight line on the storage medium. However, the cross-coupling from the x-axis on the y-axis during a scan is quite substantial, as seen in the previous section on modelling. Ideally, the feedback controller for y-axis positioning should be able to damp the micro-scanner's y-axis dynamics, shape the noise transfer function as explained above, and reduce the effect of output disturbance on the $y-$position at in-bandwidth frequencies. The last two objectives, however, are contradictory. It is straightforward to show that the two transfer functions of concern satisfy the condition

$$T_{yd}(s) = 1 + S_y(s)T_{yn}(s). \tag{9}$$

Therefore, the two transfer functions cannot be made arbitrarily small over a given frequency region. Note that $S_y(s)$, being the sensor transfer function, has a unity gain and negligible phase at in-bandwidth frequencies. The approach taken here is to use a resonant controller for the y-axis loop. The controller damps the first resonant mode of the micro-scanner in the y-axis and shapes the noise transfer function as required. However, because of condition (9), the $y-$position of the micro-scanner remains sensitive to cross-couplings from scanning along the x-axis. The fact that the controller hardly corrects for output disturbance signals at low frequencies is now utilized to reduce the effect of cross-couplings from the x-axis. Writing of servo fields is performed in two stages. In both stages the y-axis set point is kept constant. First, a line is scanned, and the y-axis position as measured by the y-axis thermal sensor is recorded. The recorded information provides an excellent estimate of the cross-coupling signal over the scanning range, and consequently, the signal $\hat{d}$ in Figure 7 can be determined as follows:

$$\hat{d}_y = \frac{d_y}{1 + K_y(s)N_y(s)P_{yy}(s)S_y(s)}. \tag{10}$$

Clearly this cross-coupling estimate is not free of sensor noise. However, it is safe to assume that the low-frequency noise component of the thermal position sensor signal during the time duration of just one scan is insignificant. The high-frequency noise can be eliminated by filtering. The same scan is then repeated by applying $\hat{d}_y$ as a feed-forward signal, as shown in Figure 7. For low-frequency scans this strategy results in minimal residual error. This procedure is then repeated for all tracks over which the servo fields are to be written. Although this procedure doubles the time needed for completion of the self servo writing process, it results in writing of self-servo fields in a satisfactory manner, as illustrated experimentally in the next section.

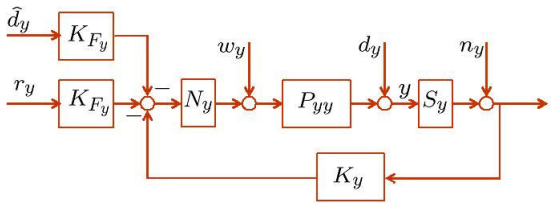

Fig. 7. Block diagram describing the feedback loop for the y-direction.

5. EXPERIMENTAL RESULTS AND DISCUSSION

The control architecture described in the previous section was implemented on a digital signal processor for both axes of the prototype storage device. The sampling time was set at 20 μs. Experimentally obtained open- and closed-loop frequency responses of the micro-scanner, for the x-axis, are plotted in Figure 8(a). Similar frequency responses obtained from simulations are plotted in Figure 8(b). There is a striking similarity between simulations and experimental results.

It can be observed, from Figure 8, that the resonant controller adds 18 dB damping to the micro-scanner's first resonant mode.

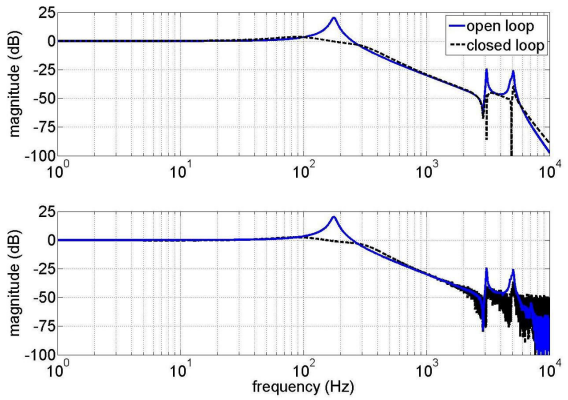

Fig. 8. Simulated (top), and experimental (bottom) open- (P_{xx}) and closed-loop (T_{xr}) transfer functions.

This amounts to shifting the open-loop pole of the micro-scanner located at $-53.7 \pm j1107.2$ to $-319.3 \pm j556.3$ and $-953.7 \pm j1661.6$ in closed loop. The increased damping improves the tracking performance significantly. In the x-direction this enables higher scan velocities and in the y-direction it mitigates the impact of transients while stepping from track to track.

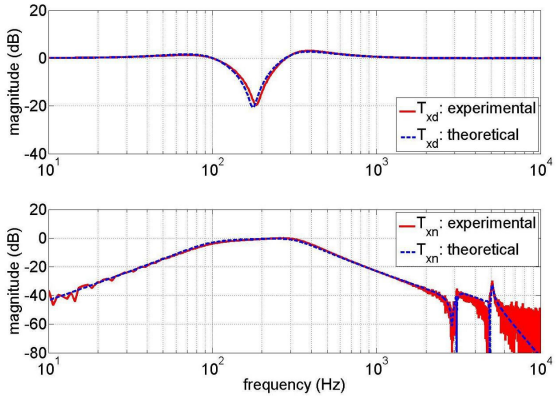

Fig. 9. The experimentally obtained T_{xd} and T_{xn} transfer functions compared with those obtained theoretically.

Figure 9 plot both the experimentally obtained and the simulated T_{xd} and T_{xn} transfer functions for the x-scan direction. There is a remarkable similarity between the simulated and experimental frequency response. The two primary attributes of this control architecture, i.e. low sensitivity to measurement noise and high sensitivity to disturbance signals, are clearly visible.

Two significant non-deterministic contributors to positioning errors while performing servo writing are sensing noise and actuator quantization noise. The 1σ sensor noise was measured to be 0.97 nm over 10 kHz. From the T_{xn} transfer function, one can estimate the impact of sensor noise on positioning, which is evaluated to be 0.21 nm 1σ (see Figure 10). The actuator noise which includes the quantization noise from the 16 bit DAC, is estimated to be 1.1 μA 1σ over 10 kHz. The impact of actuator noise is estimated using T_{xw}. It is found that the positioning error introduced is less than 0.16 nm 1σ. The net positioning error due to the stochastic components is estimated to be an astonishing 0.25 nm.

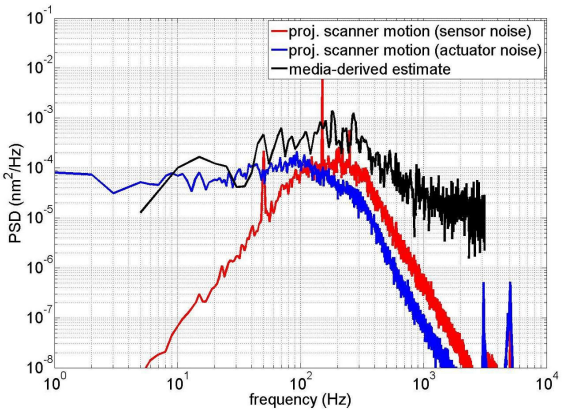

Fig. 10. Demonstration of the impact of measurement noise and actuator quantization noise on positioning resolution.

In a regular nanopositioning device, it is difficult to verify the positioning accuracy that is derived using the closed-loop transfer functions. However the nano-scale manipulation capability of the micro-cantilevers provides a unique opportunity to verify the positioning accuracy. Indentations can be formed at regular intervals using a micro-cantilever during scanning by means of the proposed control architecture. The deviations of the indentation centers from their desired locations can be measured. This provides an alternate way to characterize the positioning accuracy (see Sebastian et al. [2007]). Even though this estimate is rather noisy, the spectral characteristic of the media-derived estimate closely resembles the estimate of the positioning errors obtained from the closed-loop transfer functions (see Figure 10).

From these experiments, we can conclude that positioning errors associated with this control architecture are dominated by deterministic errors such as sensor nonlinearities and cross-coupling between axes. In a data-storage device, such as the prototype reported in this paper, errors of the latter nature are more tolerable. For example along the x-scan direction timing recovery circuits which form part of the read channel can partially correct for low-frequency positioning inaccuracies.

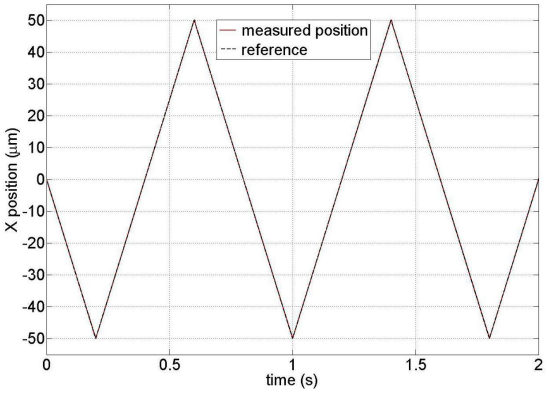

Fig. 11. Measurements obtained from x-sensor during the self servo writing operation.

The x-sensor measurement, while performing a 100 μm long scan operation is shown in Figure 11. The scan linear velocity is 0.25 nm/μs. Because of the increased damping there are no oscillations near the turn-around points.

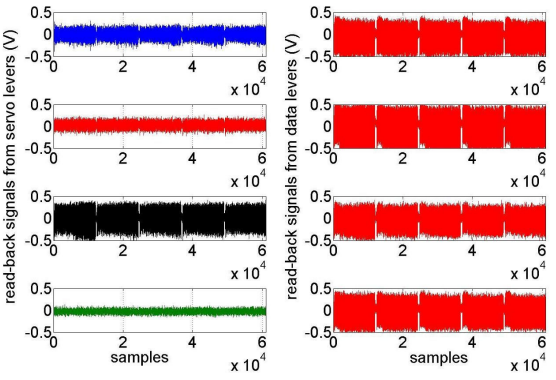

Fig. 12. Read-back signals from the four servo levers, A, B, C and D and from the four data levers.

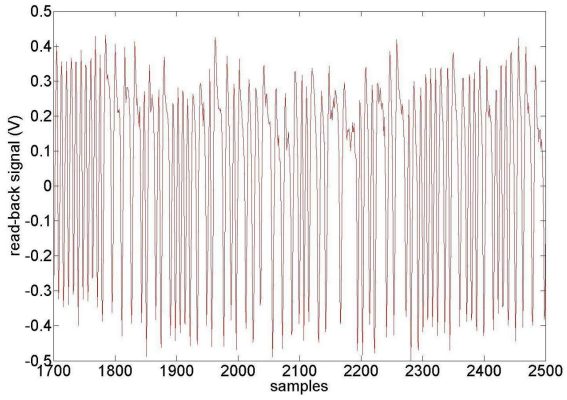

Fig. 13. Zoomed version of the signal from the data fields.

The performance of the controller is further illustrated using a complete read/write demonstration. Four micro-cantilevers were chosen to write the servo fields using the proposed control architecture. Having written the required information on the four servo fields, the PES obtained from the four servo fields were used to control the scanner using a two-sensor-based track-following control scheme reported in Pantazi et al. [2005]. The operation was performed while random data was being read from the four data levers. The data bits were recorded with an indentation pitch of 56 nm and symbol pitch of 28 nm. The read-back signals from the four servo fields and those from the data levers are shown in Figure 12. As expected the read-back signal from the C field has the maximum signal amplitude. As the data tracks are written aligned with the C field, they also show large signal amplitude. No errors were detected in over 60,000 bits. This read/write demonstration clearly shows the remarkable positioning accuracy achieved using the precisely written servo fields.

6. CONCLUSIONS

A MEMS micro-scanner with 2D motion capability is employed to position the storage medium relative to the cantilever array in a probe-based data-storage device. A pair of thermal position sensors per axis serve as global position sensors providing position information across the travel range of the micro-scanner. However, to achieve repeatable positioning over the large storage area, dedicated servo-fields are employed to obtain medium-derived position information. These servo-fields have to be written prior to operation of the device through a process known as self servo writing. Sub-nanometer positioning resolutions are needed while writing these servo-fields. Such precise positioning at acceptable bandwidth using the thermal position sensors requires directed design of the closed-loop noise sensitivity transfer function so as to minimize the impact of sensing noise. A resonant-controller-based control architecture is introduced for both x- and y- scan directions that has the desired closed-loop noise sensitivity transfer function. Experimental results are presented that show the remarkable positioning accuracies that can be achieved. The positioning error due to the actuator noise and sensing noise is estimated to be around 0.25 nm. Servo-fields are written using the proposed control architecture. Experimental write/read results based on the medium-derived position information further demonstrate the efficacy of the control scheme.

ACKNOWLEDGEMENTS

We thank our colleagues of the Probe Storage Group at the IBM Zurich Research Laboratory. Special thanks go to M. Despont, U. Drechsler, M. Lantz, and H. Rothuizen for the design and fabrication of MEMS parts, to D. Jubin for the characterization and assembly of the MEMS components, and to P. Bächtold for the design of the electronics used in this work.

REFERENCES

E. Eleftheriou, T. Antonakopoulos, G. K. Binnig, G. Cherubini, M. Despont, A. Dholakia, U. Dürig, M. A. Lantz, H. Pozidis, H. E. Rothuizen, and P. Vettiger. Millipede-a MEMS based scanning-probe data storage system. *IEEE Transactions on Magnetics*, 39(2):938–945, 2003.

D. Halim and S. O. R. Moheimani. Spatial resonant control of flexible structures - application to a piezoelectric laminate beam. *IEEE Transactions on Control Systems Technology*, 9 (1):37–53, January 2001.

M. A. Lantz, G. K. Binnig, M. Despont, and U. Drechsler. A micromechanical thermal displacement sensor with nanometer resolution. *Nanotechnology*, 16:1089–1094, May 2005.

M. A. Lantz, H. Rothuizen, U. Drechsler, W. Haeberle, and M. Despont. A vibration resistant nanopositioner for mobile parallel-probe storage applications. *Journal of Microelectromechanical Systems*, 16(1):130–139, February 2007.

S. O. R. Moheimani and B. J. G. Vautier. Resonant control of structural vibration using charge-driven piezoelectric actuators. *IEEE Transactions on Control Systems Technology*, 13 (6):1021–1035, 2005.

A. Pantazi, A. Sebastian, G. Cherubini, M. Lantz, H. Pozidis, H. Rothuizen, and E. Eleftheriou. Control of MEMS-based scanning-probe data-storage devices. *IEEE Transactions on Control System Technology*, 15(5):824–841, September 2007.

A. Pantazi, A. Sebastian, H. Pozidis, and E. Eleftheriou. Two-sensor-based H_∞ control for nanopositioning in probe storage. In *Proceedings of the IEEE Conference on Decision and Control, Seville, Spain*, pages 1174–1179, December 2005.

H. R. Pota, S. O. R. Moheimani, and M. Smith. Resonant controllers for smart structures. *Smart Materials and Structures*, 11(1):1–8, 2002.

A. Sebastian, A. Pantazi, and H. Pozidis. Jitter investigation and performance evaluation of a small-scale probe storage device prototype. In *Proceedings of the IEEE Global Communications Conference*, pages 288–293, November 2007.